

# Vortex Transport and Pinning Effectiveness in Conformal Pinning Arrays

D. Ray<sup>1,2</sup>, C. Reichhardt<sup>2</sup>, C. J. Olson Reichhardt<sup>2</sup>, and B. Jankó<sup>1</sup>

<sup>1</sup>*Department of Physics, University of Notre Dame, Notre Dame, Indiana 46556, USA*

<sup>2</sup>*Theoretical Division, Los Alamos National Laboratory, Los Alamos, New Mexico 87545, USA*

---

## Abstract

We examine the current driven dynamics for vortices interacting with conformal crystal pinning arrays and compare to the dynamics of vortices driven over random pinning arrays. We find that the pinning is enhanced in the conformal arrays over a wide range of fields, consistent with previous results from flux gradient-driven simulations. At fields above this range, the effectiveness of the pinning in the moving vortex state can be enhanced in the random arrays compared to the conformal arrays, leading to crossing of the velocity-force curves.

*Key words:* vortex, conformal pinning, dynamics

---

## 1. Introduction

Many of the applications of type-II superconductors require that the system maintain a large critical current or effective pinning of vortices in the presence of a magnetic field [1]. One approach to this problem is the use of lithography to create arrays of artificial pinning sites [2–6] by means of nanohole lattices [2–5] or arrays of magnetic dots [6]. This raises the question of what arrangement of pinning sites maximizes the effectiveness of the pinning, for a given number of sites. In periodic arrays of pinning sites, strong commensuration or matching effects can occur when the number of vortices equals an integer multiple  $n$  of the number of pinning sites [2,3,7,8]. At the matching conditions, there can be a peak in the critical current when the vortices form an ordered state [3,7,8]. The enhancement of pinning at commensurate fields has also been observed in colloidal experiments [9] on periodic optical trap arrays. The colloids are repulsively interacting particles that have behavior similar to that of vortices, showing that understanding vortex

dynamics on periodic or semi-periodic substrates is also useful for the general understanding of dynamics near commensurate-incommensurate transitions [10]. For fields close to matching fields, interstitials or vacancies can appear in the ordered vortex structure and act as effective particles that are weakly pinned [11]. However, away from the matching fields, the critical current falls off substantially and the pinning becomes less effective.

Other approaches to pinning enhancement include the use of quasiperiodic pinning arrays such as Penrose tilings [12–14]. Commensuration effects still occur for such arrays; moreover, the strength of the pinning at nonmatching fields is generally improved from that found for nonmatching fields in periodic or random pinning arrays [12,13]. The random dilution of periodic pinning arrays produces peaks in the critical current not only at the matching fields but also at fields where the number of vortices matches the number of pinning sites in the original undiluted array [15]. Strong non-integer matching peaks in the critical current also appear in honeycomb pinning arrays, which are an example

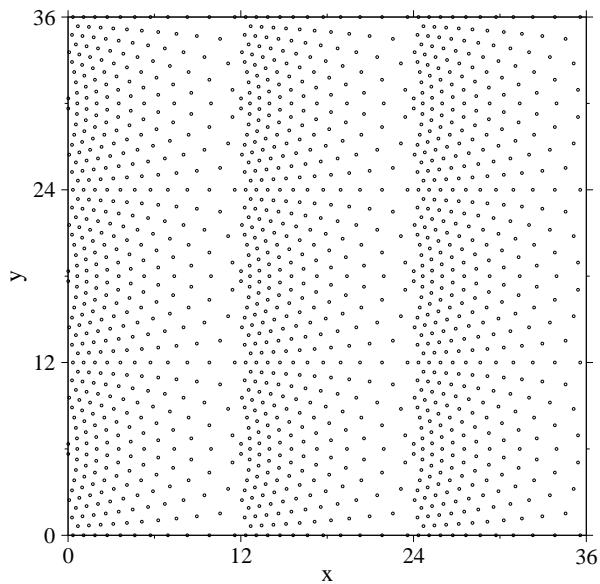


Fig. 1. The conformal pinning geometry used for simulated transport measurements. A random pinning array with the same number of pins is used for comparison (not shown). Periodic boundary conditions apply in both the  $x$ - and  $y$ -directions. The drive is applied in the positive  $x$ -direction.

of an ordered diluted triangular pinning array [16]. Enhancement of the pinning at fractional fields can be achieved using artificial ice pinning array geometries [17], and these fractional matching peaks can be as strong as or even stronger than the integer matching peaks [18].

All the previously mentioned approaches have the deficiency of exhibiting reduced pinning effectiveness away from certain special field values. To address this issue, a new type of pinning geometry called a conformal crystal pinning array (illustrated in Fig. 1) was recently proposed [19]. This array is constructed by performing a conformal transformation [20] on a triangular lattice to create a gradient in the pinning density while preserving the local sixfold ordering of the original triangular array. Flux gradient simulations show that the overall critical current in the conformal pinning array (CPA) is enhanced over that of a uniform random pinning array [19] for a wide range of fields, and is also higher than that of uniform periodic pinning arrays except for fields very close to integer matching, where the periodic pinning gives a marginally higher critical current. The gradient in pinning density present in the CPA enhances the pinning since it can match the gradient in the vortex density, and also leads to an absence of commensuration effects or peaks in the critical current. Random pinning arrays with

a density gradient equivalent to that of the CPA produce a small critical current enhancement compared to uniform random arrays; however, a CPA with the same number of pinning sites gives a substantially larger critical current, indicating that the preservation of the sixfold ordering of the pinning array is also important for enhancing the pinning [19]. The simulation predictions were subsequently confirmed in experiments which compared CPAs to random and periodic arrays [21,22]. Other work on non-conformal pinning arrays containing gradients includes numerical studies of hyperbolic tessellations [23], as well as experiments on non-conformal pinning arrays with gradients in which the pinning was enhanced compared to uniform arrays [24].

The first numerical work on CPAs focused on flux-gradient driven simulations where the critical current is proportional to the width of the magnetization loop [19]. In such simulations, there is a gradient in the vortex density across the sample [25]. One question is whether the CPA still produces enhanced pinning in systems driven with an applied current. Previous work indicated that the CPA produces a pinning enhancement compared to random arrays in this case as well [19]. In this work we further explore the current-driven system by varying the applied magnetic field and analyzing the vortex velocity as a function of external drive to produce a measurement that is proportional to an experimentally measurable voltage-current curve. We find that at very low vortex densities, the difference in critical current between random arrays and CPAs is small, and that as the field increases, the conformal arrays have stronger effective pinning, producing both a larger depinning force and a lower average vortex velocity in the moving state compared to random arrays. At higher fields, the CPA still has a high depinning threshold; however, once the vortices are in the moving state, the average vortex velocity for the random arrays can be lower than that for the CPA, indicating that the effectiveness of the pinning in the dynamic regime is suppressed for the CPA compared to the random pinning. We show that this arises due to the earlier onset of dynamical ordering [26,27] in CPAs compared to random pinning arrays at these higher magnetic fields.

## 2. Simulations

We consider an effective 2D model of pointlike vortices where a single vortex  $i$  obeys the following

equation of motion:

$$\eta \frac{d\mathbf{R}_i}{dt} = \mathbf{F}_i^{vv} + \mathbf{F}_i^P + \mathbf{F}_i^D. \quad (1)$$

Here  $\eta = \phi_0^2 d / 2\pi \xi^2 \rho_N$  is the damping constant,  $d$  is the sample thickness,  $\phi_0 = h/2e$  is the elementary flux quantum, and  $\rho_N$  is the normal-state resistivity of the material; we work in units where  $\eta$  is set equal to 1. Vortex  $i$  is located at  $\mathbf{R}_i$ . The vortex-vortex repulsive interaction force is  $\mathbf{F}_i^{vv} = \sum_{j \neq i}^{N_v} F_0 K_1(R_{ij}/\lambda) \hat{\mathbf{R}}_{ij}$ , where  $K_1$  is the modified Bessel function,  $\lambda$  is the London penetration depth,  $F_0 = \phi_0^2 / (2\pi \mu_0 \lambda^3)$ ,  $R_{ij} = |\mathbf{R}_i - \mathbf{R}_j|$  is the distance between vortex  $i$  and vortex  $j$ , and the unit vector  $\hat{\mathbf{R}}_{ij} = (\mathbf{R}_i - \mathbf{R}_j)/R_{ij}$ . The force from the pinning sites is given by  $\mathbf{F}_i^P$ . Various models for the pinning can be considered; here, we use parabolic attractive sites with

$$\mathbf{F}_i^P = - \sum_{k=1}^{N_p} (F_p/r_p) (\mathbf{R}_i - \mathbf{R}_k^{(p)}) \Theta[r_p - |\mathbf{R}_i - \mathbf{R}_k^{(p)}|], \quad (2)$$

where  $\mathbf{R}_k^{(p)}$  is the location of pinning site  $k$ ,  $F_p$  is the maximum pinning force,  $r_p$  is the pinning radius, and  $\Theta$  is the Heaviside step function. Finally, an externally applied current  $\mathbf{J}$  produces a Lorentz force  $\mathbf{F}_i^D = \mathbf{J} \times \mathbf{B}$  on the vortices that is perpendicular to the applied current.

To measure the transport properties of a given pinning array, we first place  $N_v$  vortices randomly and allow them to anneal; then we apply a slowly increasing driving force  $\mathbf{F}^D = F_d \hat{\mathbf{x}}$  in the  $x$  direction and measure the resulting average vortex velocity in the  $x$  direction,  $\langle v_x \rangle = (1/N_v) \sum_{i=1}^{N_v} \mathbf{v}_i \cdot \hat{\mathbf{x}}$ , where  $\mathbf{v}_i = d\mathbf{R}_i/dt$ . The system geometry is illustrated in Fig. 1, where we show a conformal pinning array. The construction of the CPA is described in [19]. Transport measurements were also performed with an array of randomly distributed pinning sites for comparison. In both arrays, the pinning density is maintained at  $n_p = 1.0/\lambda^2$  with pinning radius  $r_p = 0.12\lambda$  and pinning force  $F_p = 0.55F_0$ . Simulations performed with these parameter choices should be in the same regime as recently conducted experiments on CPAs [21,22]. The system size is  $36\lambda \times 36\lambda$ , with periodic boundary conditions in the  $x$ - and  $y$ -directions. In this work, we characterize transport as a function of the number of vortices  $N_v$ ; we report this number as  $B/B_\phi = N_v/1296$ , where  $B$  is the average magnetic field in the sample resulting from the vortices and  $B_\phi$  is the matching field achieved

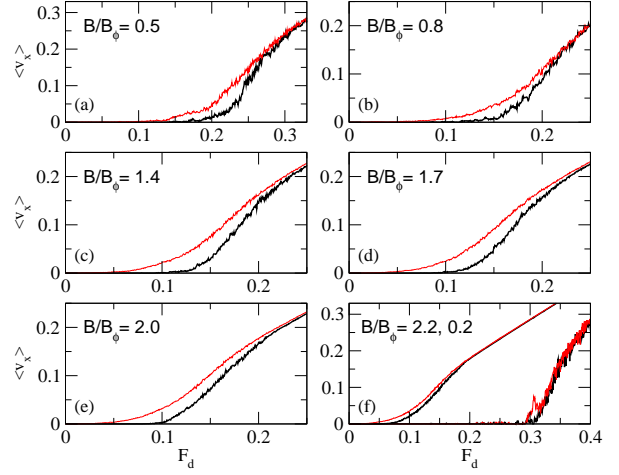


Fig. 2.  $\langle v_x \rangle$  versus  $F_d$  curves for the CPA (lower dark lines) and random arrays (upper light lines) for  $B/B_\phi =$  (a) 0.5, (b) 0.8, (c) 1.4, (d) 1.7, (e) 2.0, and (f) 0.2 (right lines) and 2.2 (left lines). Panels (a-e) show that the effectiveness of the pinning for the CPA is higher than for the random array over a wide range of fields. Panel (f) shows field levels at the extremes of this range, where the CPA is no longer more effective than random pinning.

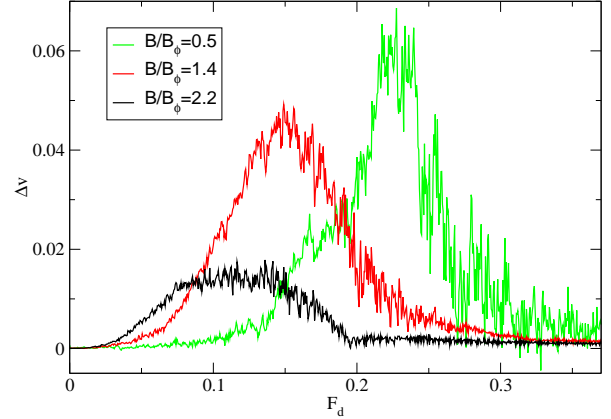


Fig. 3. The difference between the velocity response in the random array and the CPA,  $\Delta v = \langle v_x^{\text{rand}} \rangle - \langle v_x^{\text{CPA}} \rangle$ , vs  $F_d$  for samples with  $B/B_\phi = 0.5, 1.4$ , and  $2.2$  (upper right to lower left). In this field range,  $\Delta v$  is positive, indicating that the pinning is more effective in the CPA at low and intermediate values of  $F_d$ . At the highest drives, the response of both arrays becomes Ohmic and  $\Delta v$  goes to zero.

when the number of vortices equals the number of pinning sites.

### 3. Transport

In Fig. 2 we plot  $\langle v_x \rangle$  versus  $F_d$  for uniform random arrays and CPAs at fields ranging from  $B/B_\phi = 0.2$  to  $2.2$ . Panels (a-e) show that over a wide range

of fields from 0.5 to 2.0, vortices consistently remain stationary or pinned up to a higher drive in the CPA than in the random array, providing evidence that the pinning in the CPA is more effective than in the random array. This range of fields where we see increased CPA effectiveness in transport simulations is consistent with the corresponding range found for magnetization using quasistatic flux-gradient driven simulations in [19]. Moreover, even above the depinning threshold, vortices continue to move more slowly through the CPA; we show this explicitly in Fig. 3 where we plot the difference between the velocity response in the random array and the CPA,  $\Delta v = \langle v_x^{\text{rand}} \rangle - \langle v_x^{\text{CPA}} \rangle$ , as a function of  $F_d$ . We see that the pinning in the CPA is more effective than in the random array, with a positive  $\Delta v$  for all but the highest values of  $F_d$ .

In panel (f) of Fig. 2, we explore field values at the edges of the range, where the CPA loses its increased effectiveness. At a low field level,  $B/B_\phi = 0.2$ , the transport curves lie on top of each other. Because there are so few vortices present in the system, only a small percentage of the pinning sites in an array are actually pinning vortices at any given time. The pinning arrays are being very sparsely sampled, and so the details of their structure do not come into play. Conversely, at a high field level  $B/B_\phi = 2.2$ , the dense packing of vortices in the system begins to overwhelm the pinning. The CPA has a spatially varying density of pinning sites; in the gradient-driven simulations of [19], it was shown that the CPA begins to fail when the vortex density exceeds the maximum density of pinning sites, which occurs at one edge of the CPA (corresponding to  $x = 0\lambda, 12\lambda, 24\lambda$  in Fig. 1). The CPA used in this work has a maximum pinning density of  $2.0\lambda^{-2}$ , so this explanation is consistent with our results.

Fig. 3 brings out this trend of decreased CPA effectiveness at high fields. For example, we can examine the maximum  $\Delta v$  achieved: at  $B/B_\phi = 1.4$ ,  $\Delta v$  reaches a maximum value of 0.045, while for  $B/B_\phi = 2.2$  the maximum value of  $\Delta v$  is only 0.015, indicating that as  $B/B_\phi$  increases, the difference in pinning effectiveness of the CPA compared to the random pinning array is reduced. We can also look at the transition to the Ohmic regime which occurs for large  $F_d$ , where  $\Delta v$  goes to 0 as all the vortices flow freely in response to the large driving force, and the effects of the pinning become minimal. The transition to the Ohmic response regime occurs near  $F_d = 0.26$  for  $B/B_\phi = 1.4$  in Fig. 3, while for  $B/B_\phi = 2.2$ , the transition drops to a lower value of  $F_d = 0.19$ .

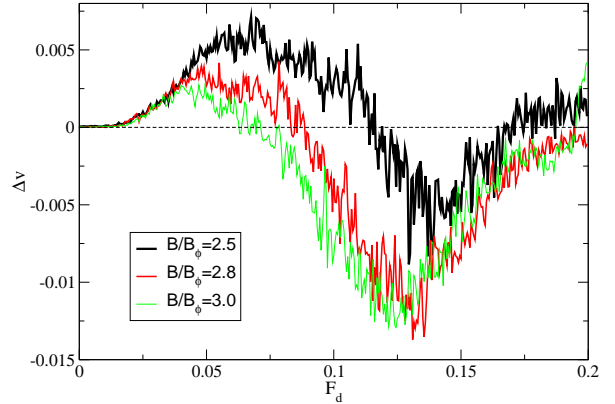


Fig. 4.  $\Delta v$  vs  $F_d$  for samples with high field values of  $B/B_\phi = 2.5, 2.8$ , and  $3.0$  (upper right to lower left). For low  $F_d$ , the pinning is more effective in the CPA, as indicated by the positive value of  $\Delta v$ ; however, at intermediate  $F_d$ , the pinning becomes more effective in the random arrays as shown by the negative  $\Delta v$ .

#### 4. CPA Breakdown

If we consider even higher field values, then a new feature arises in the velocity-force curves. In Fig. 4 we plot the quantity  $\Delta v$  defined in the previous section for  $B/B_\phi = 2.5, 2.8$ , and  $3.0$ . For each of these fields  $\Delta v$  is initially positive, but drops below zero as  $F_d$  increases, indicating that the average vortex velocity is higher in the CPA than in the random array at intermediate values of  $F_d$ , so that CPA pinning actually becomes less effective than random pinning. The reversal of the effectiveness of the pinning in the moving state produces a crossing in the velocity vs force curves, as shown in panel (c) of Fig. 5 ( $B/B_\phi = 2.8$ ) compared to panels (a-b) ( $B/B_\phi = 1.7, 2.2$ ).

The reversal of the effectiveness in the pinning at intermediate drives occurs because the vortices dynamically order or partially crystallize at a lower drive in the CPA than in the random pinning array. It is known from current-driven simulation studies of random pinning arrays that a dynamical reordering transition can occur into a moving state that is partially crystalline or smectic-like [26,27]. In the dynamically ordered state, the vortex velocities are generally higher than in moving states with more random ordering, since the shear modulus of a random structure is much lower. A disordered vortex configuration has a higher probability of some vortices being temporarily pinned by the substrate, while in a moving crystal state, the vortices all move together and can not be individually trapped by pinning sites. For the random array, as the field in-

creases, the drive  $F_d^{Or}$  at which the vortices begin to dynamically order decreases.  $F_d^{Or}$  is also a function of the pinning density  $n_p$ , and as  $n_p$  decreases,  $F_d^{Or}$  also decreases. In the CPA, the pinning density has a gradient, and as a result, there is a gradient in the value of  $F_d^{Or}$  across the sample. At the higher magnetic fields, the vortices can start to locally dynamically order in the lower pin density portions of the CPA sample.

The partially ordered state forms in the low pin density regions during a transient time  $\tau_o$ , and this state becomes disordered while passing through the high pin density regions during a transient time  $\tau_d$ . As the field increases, these transient times change, and the vortices remain disordered if  $\tau_d > \tau_o$ , while for  $\tau_o < \tau_d$  the vortices can order. This means that in a random pinning array, the vortices are disordered when  $F_d < F_d^{Or}$ ; however, for a CPA at the same value of  $F_d$ , if  $\tau_o < \tau_d$ , an ordered moving vortex state will form and hence  $v_x$  for the CPA will be higher than for the random array. As  $B/B_\phi$  increases,  $\tau_o$  decreases. This is consistent with the behavior in Fig. 4, where the extent of the range of  $F_d$  over which  $\Delta v < 0$  grows as  $B/B_\phi$  increases. It may be possible that at high enough  $B/B_\phi$ , the vortices in the CPA would immediately dynamically order as soon as they depin; in this case, the critical current for the random array would be higher than that of the CPA.

In Fig. 5 we plot simultaneously  $\langle v_x \rangle$  and the fraction of six-fold coordinated vortices  $P_6$  versus  $F_d$  for the random pinning and the CPA. In the dynamically ordered moving crystal state,  $P_6$  is close to 1 [26,27]. In Fig. 5(a) at  $B/B_\phi = 1.7$ , the pinning is more effective in the CPA over the entire window of  $F_d$  shown in the figure. At depinning,  $P_6$  drops for both types of pinning as the system enters a plastic flow regime. At higher  $F_d$ ,  $P_6$  increases when the vortices begin to reorder, and in Fig. 5(a),  $P_6$  for the random array is higher than that for the CPA for  $F_d > 0.15$ . In Fig. 5(b) for  $B/B_\phi = 2.2$ , we find a similar trend; however, in Fig. 5(c) for  $B/B_\phi = 2.8$ ,  $P_6$  is higher for the CPA than for the random array for  $F_d > 0.1$ . This also corresponds to the range of  $F_d$  over which  $\langle v_x \rangle$  in the CPA is higher than in the random array. At  $F_d = 0.2$ ,  $P_6$  reaches nearly the same value for both arrays, and the difference in  $\langle v_x \rangle$  between the two arrays also vanishes. This result confirms that at high magnetic fields, the vortices dynamically order at a lower drive for the CPA than for a random pinning array.

We can roughly estimate the relative effective-

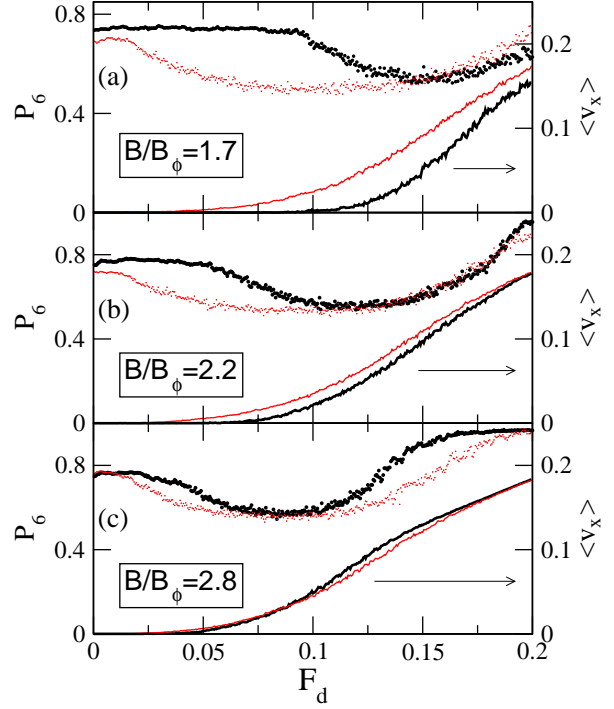


Fig. 5. Lower solid curves:  $\langle v_x \rangle$  vs  $F_d$  for a random array (light lines) and a CPA (dark lines). Upper symbols:  $P_6$ , the fraction of sixfold coordinated vortices, vs  $F_d$  for a random array (light symbols) and a CPA (dark symbols). (a)  $B/B_\phi = 1.7$ . (b)  $B/B_\phi = 2.2$ . (c)  $B/B_\phi = 2.8$ . In (c), the vortices dynamically order at a lower drive for the CPA than for the random array, giving a lower value of  $\langle v_x \rangle$  for the random array at the intermediate drives  $0.1 < F_d < 0.2$ .

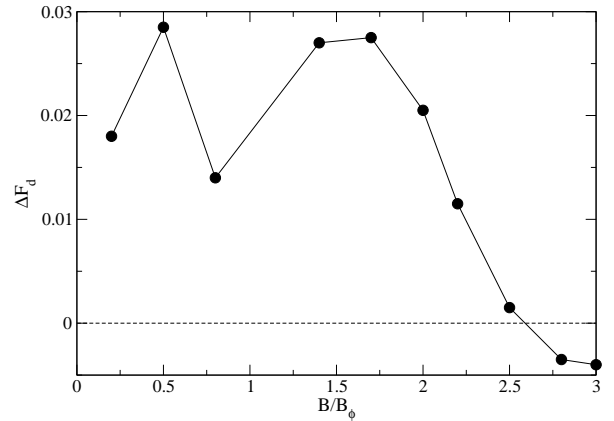


Fig. 6. The difference in the external drive  $F_d$  at which  $\langle v_x \rangle = 0.05$  between the random and the conformal arrays,  $\Delta F_d = F_d^{\text{rand}}(\langle v_x \rangle = 0.05) - F_d^{\text{CPA}}(\langle v_x \rangle = 0.05)$ , vs  $B/B_\phi$ . At low fields,  $\Delta F_d$  is small, at intermediate fields the CPA has stronger pinning ( $\Delta F_d > 0$ ), and for  $B/B_\phi > 2.5$  the random array has stronger pinning ( $\Delta F_d < 0$ ).

ness of the pinning in the CPA and random pinning arrays by plotting the difference in the value  $F_d$  at which  $\langle v_x \rangle = 0.05$  for the two arrays,  $\Delta F_d = F_d^{\text{rand}}(\langle v_x \rangle = 0.05) - F_d^{\text{CPA}}(\langle v_x \rangle = 0.05)$ . Figure 6 shows that at low  $B/B_\phi$ ,  $\Delta F_d$  is small and the difference between the random and conformal array is minimal due to the weak vortex-vortex interactions.  $\Delta F_d$  is large and positive over the range  $0.5 < B/B_\phi < 2.0$ ; it then decreases and becomes negative for  $B/B_\phi > 2.5$ . While the exact value of  $B/B_\phi$  at which  $\Delta F_d$  drops below zero will depend on the velocity value chosen for the measurement, Fig. 6 is consistent with the idea that the CPA is highly effective at fields less than the maximum local pinning density of the CPA, but falls off in effectiveness above this value. It should be noted that the CPA effectiveness may also depend on the size  $r_p$  and strength  $F_p$  of the pinning sites, both of which can be sample dependent.

## 5. Summary

We investigated the current driven dynamics of vortices interacting with conformal pinning arrays and compared the effectiveness of the pinning to that of random pinning arrays with the same total number of pinning sites. The conformal pinning array is constructed by performing a conformal transformation of a triangular pinning array to create a new pinning array that has a density gradient but still conserves the local sixfold ordering of the original triangular array. We find that for vortex densities not exceeding the maximum local density of pinning sites in the conformal array, the critical depinning force for the conformal array is higher than that of the random array; and furthermore, in the moving vortex state, the velocity of the vortices in the conformal array is lower than in the random array. At higher fields, the critical depinning force for the conformal array remains higher than that of the random array, but at intermediate drives the average vortex velocity in the random arrays becomes lower than that in the conformal array, leading to a crossing of the velocity-force curves. This reversal of the pinning effectiveness arises because the vortices dynamically order at a lower drive in the conformal array than in the random array. Finally, at high drives, the difference between the two types of arrays is washed out due to dynamical reordering of the vortices.

There are still issues to consider in the conformal

pinning array, such as performing conformal transformations on lattice structures other than a triangular array. It would also be interesting to investigate vortex ratchet effects of the type previously found in samples with random or periodic pinning arrays [28,29], as these effects

This work was carried out under the auspices of the NNSA of the U.S. DoE at LANL under Contract No. DE-AC52-06NA25396.

## References

- [1] M. Tinkham, *Introduction to Superconductivity* (McGraw-Hill, New York, 1975); G. Blatter, M.V. Feigelman, V.B. Geshkenbein, A.I. Larkin, V.M. Vinokur, Rev. Mod. Phys. 66 (1994) 1125.
- [2] M. Baert, V.V. Metlushko, R. Jonckheere, V.V. Moshchalkov, Y. Bruynseraede, Phys. Rev. Lett. 74 (1995) 3269; Europhys. Lett. 29 (1995) 157.
- [3] K. Harada, O. Kamimura, H. Kasai, T. Matsuda, A. Tonomura, V.V. Moshchalkov, Science 274 (1996) 1167.
- [4] U. Welp, Z.L. Xiao, J.S. Jiang, V.K. Vlasko-Vlasov, S.D. Bader, G.W. Crabtree, J. Liang, H. Chik, J.M. Xu, Phys. Rev. B 66 (2002) 212507.
- [5] A.N. Grigorenko, S.J. Bending, M.J. Van Bael, M. Lange, V.V. Moshchalkov, H. Fangohr, P.A.J. de Groot, Phys. Rev. Lett. 90 (2003) 237001; A.D. Thakur, S. Ooi, S.P. Chockalingam, J. Jesudasan, P. Raychaudhuri, K. Hirata, Appl. Phys. Lett. 94 (2009) 262501; I. Swiecicki, C. Ulysse, T. Wolf, R. Bernard, N. Bergeal, J. Briatico, G. Faini, J. Lesueur, J.E. Villegas, Phys. Rev. B 85 (2012) 224502.
- [6] J.I. Martín, M. Vélez, J. Nogués, I.K. Schuller, Phys. Rev. Lett. 79 (1997) 1929; M.J. Van Bael, K. Temst, V.V. Moshchalkov, Y. Bruynseraede, Phys. Rev. B 59 (1999) 14674.
- [7] C. Reichhardt, C. J. Olson, F. Nori, Phys. Rev. B 57 (1998) 7937.
- [8] G.R. Berdiyrov, M.V. Milosevic, F.M. Peeters, Europhys. Lett. 74 (2006) 493; Phys. Rev. B 74 (2006) 174512.
- [9] T. Bohlein, J. Mikhael, C. Bechinger, Nat. Mater. 11 (2012) 126.
- [10] C. Reichhardt, C.J. Olson Reichhardt, Phys. Rev. E 79 (2009) 061403; A. Vanossi, N. Manini, E. Tosatti, Proc. Natl. Acad. Sci. USA 109 (2012) 16429; D. McDermott, J. Amelang, C.J. Olson Reichhardt, C. Reichhardt, Phys. Rev. E 88 (2013) 062301.
- [11] C. Reichhardt, C.J. Olson, F. Nori, Phys. Rev. Lett. 78 (1997) 2648; C. Reichhardt, G.T. Zimányi, Niels Grønbech-Jensen, Phys. Rev. B 64 (2001) 014501.
- [12] V. Misko, S. Savelev, F. Nori, Phys. Rev. Lett. 95 (2005) 177007.
- [13] M. Kemmler, C. Gürlich, A. Sterck, H. Pöhler, M. Neuhaus, M. Siegel, R. Kleiner, and D. Koelle, Phys. Rev. Lett. 97 (2006) 147003; A.V. Silhanek, W. Gillijns, V.V. Moshchalkov, B.Y. Zhu, J. Moonens, and L.H.A. Leunissen, Appl. Phys. Lett. 89 (2006) 152507.

- [14] C. Reichhardt, C.J. Olson Reichhardt, Phys. Rev. Lett. 106 (2011) 060603.
- [15] C. Reichhardt, C. J. Olson Reichhardt, Phys. Rev. B 76 (2007) 094512. M. Kemmler, D. Bothner, K. Ilin, M. Siegel, R. Kleiner, D. Koelle, Phys. Rev. B 79 (2009) 184509.
- [16] C. Reichhardt, C.J. Olson Reichhardt, Phys. Rev. B 76 (2007) 064523; R. Cao, L. Horng, T.C. Wu, J.C. Wu, T.J. Yang, J. Phys.: Condens. Matter 21 (2009) 075705.
- [17] A. Libál, C.J. Olson Reichhardt, C. Reichhardt, Phys. Rev. Lett. 102 (2009) 237004; J. Trastoy, M. Malnou, C. Ulysse, R. Bernard, N. Bergeal, G. Faini, J. Lesueur, J. Briatico, J.E. Villegas, arXiv:1307.2881.
- [18] M.L. Latimer, G.R. Berdiyrov, Z.L. Xiao, F.M. Peeters, W.K. Kwok, Phys. Rev. Lett. 111 (2013) 067001.
- [19] D. Ray, C.J. Olson Reichhardt, B. Jankó, C. Reichhardt, Phys. Rev. Lett. 110 (2013) 267001.
- [20] F. Rothen, P. Pieranski, Phys. Rev. E 53 (1996) 2828.
- [21] Y.L. Wang, M.L. Latimer, Z.L. Xiao, R. Divan, L.E. Ocola, G.W. Crabtree, W.K. Kwok, Phys. Rev. B 87 (2013) 220501.
- [22] S. Guéron, Y.J. Rosen, A.C. Basaran, I.K. Schuller, Appl. Phys. Lett. 102 (2013) 252602.
- [23] V.R. Misko, F. Nori, Phys. Rev. B 85 (2012) 184506.
- [24] M. Motta, F. Colauto, W.A. Ortiz, J. Fritzsche, J. Cuppens, W. Gillijns, V.V. Moshchalkov, T.H. Johansen, A. Sanchez, A.V. Silhanek, Appl. Phys. Lett. 102 (2013) 212601.
- [25] C. Reichhardt, C.J. Olson, J. Groth, S. Field, F. Nori, Phys. Rev. B 52 (1995) 10441; C. Reichhardt, J. Groth, C.J. Olson, S.B. Field, F. Nori, Phys. Rev. B 54 (1996) 16108.
- [26] A.E. Koshelev and V.M. Vinokur, Phys. Rev. Lett. 73 (1994) 3580.
- [27] C.J. Olson, C. Reichhardt, F. Nori, Phys. Rev. Lett. 81 (1998) 3757.
- [28] C.J. Olson, C. Reichhardt, B. Jankó, F. Nori, Phys. Rev. Lett. 87 (2001) 177002.
- [29] W. Gillijns, A.V. Silhanek, V.V. Moshchalkov, C.J. Olson Reichhardt, C. Reichhardt, Phys. Rev. Lett. 99 (2007) 247002.